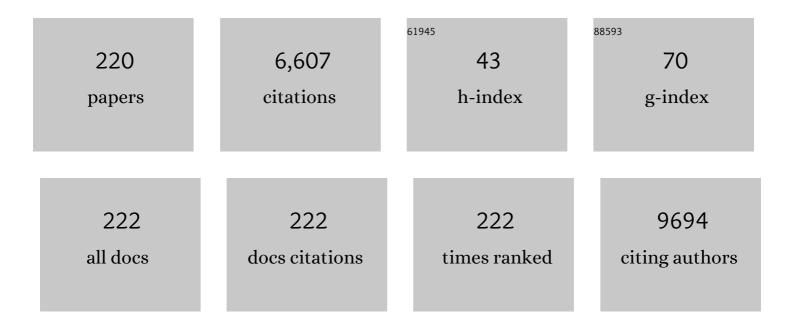
## Zheng Jun Zhang

List of Publications by Year in descending order

Source: https://exaly.com/author-pdf/1786033/publications.pdf Version: 2024-02-01



#	Article	IF	CITATIONS
1	Pyridinicâ€Nitrogenâ€Ðominated Graphene Aerogels with Fe–N–C Coordination for Highly Efficient Oxygen Reduction Reaction. Advanced Functional Materials, 2016, 26, 5708-5717.	7.8	360
2	Openâ€Ended, Nâ€Doped Carbon Nanotube–Graphene Hybrid Nanostructures as Highâ€Performance Catalyst Support. Advanced Functional Materials, 2011, 21, 999-1006.	7.8	358
3	Nanostructured VO <sub>2</sub> Photocatalysts for Hydrogen Production. ACS Nano, 2008, 2, 1492-1496.	7.3	162
4	Emergence of Kondo lattice behavior in a van der Waals itinerant ferromagnet, Fe <sub>3</sub> GeTe <sub>2</sub> . Science Advances, 2018, 4, eaao6791.	4.7	157
5	Reduced graphene oxide/carbon nanotube hybrid film as high performance negative electrode for supercapacitor. Electrochimica Acta, 2015, 169, 342-350.	2.6	139
6	Surface-Enhanced Raman Scattering Detection of Pesticide Residues Using Transparent Adhesive Tapes and Coated Silver Nanorods. ACS Applied Materials & Interfaces, 2018, 10, 9129-9135.	4.0	130
7	Oxygen vacancy–induced ferromagnetism in un-doped ZnO thin films. Journal of Applied Physics, 2012, 111, .	1.1	125
8	Surface Plasmon Enhanced Photocatalysis of Au/Pt-decorated TiO2 Nanopillar Arrays. Scientific Reports, 2016, 6, 26670.	1.6	119
9	Tuning the Field-Emission Properties of Tungsten Oxide Nanorods. Small, 2005, 1, 310-313.	5.2	116
10	Plasmon-mediated photothermal and superhydrophobic TiN-PTFE film for anti-icing/deicing applications. Composites Science and Technology, 2019, 181, 107696.	3.8	105
11	Enhanced photoelectrochemical and photocatalytic performance of TiO2 nanorod arrays/CdS quantum dots by coating TiO2 through atomic layer deposition. Nano Energy, 2015, 11, 400-408.	8.2	104
12	Rapid, low-temperature synthesis of single-crystalline Co <sub>3</sub> O <sub>4</sub> nanorods on silicon substrates on a large scale. Nanotechnology, 2008, 19, 155606.	1.3	97
13	Morphological influence of TiO 2 nanostructures (nanozigzag, nanohelics and nanorod) on photocatalytic degradation of organic dyes. Applied Surface Science, 2017, 400, 184-193.	3.1	95
14	Silver Nanorods Wrapped with Ultrathin Al2O3 Layers Exhibiting Excellent SERS Sensitivity and Outstanding SERS Stability. Scientific Reports, 2015, 5, 12890.	1.6	89
15	Visible light assisted photocatalytic degradation of crystal violet dye and electrochemical detection of ascorbic acid using a BiVO <sub>4</sub> /FeVO <sub>4</sub> heterojunction composite. RSC Advances, 2018, 8, 23489-23498.	1.7	86
16	NiO films consisting of vertically aligned cone-shaped NiO rods. Applied Physics Letters, 2006, 88, 033101.	1.5	83
17	Optical and dielectric properties of a nanostructured NbO2 thin film prepared by thermal oxidation. Journal Physics D: Applied Physics, 2004, 37, 3392-3395.	1.3	82
18	Melting and optical properties of ZnO nanorods. Applied Physics Letters, 2006, 88, 061913.	1.5	81

#	Article	IF	CITATIONS
19	Arrays of aligned, single crystalline silver nanorods for trace amount detection. Journal Physics D: Applied Physics, 2008, 41, 152007.	1.3	81
20	Hybridized plasmon modes and near-field enhancement of metallic nanoparticle-dimer on a mirror. Scientific Reports, 2016, 6, 30011.	1.6	80
21	Ultrasensitive Fieldâ€Effect Biosensors Enabled by the Unique Electronic Properties of Graphene. Small, 2020, 16, e1902820.	5.2	75
22	Intense photoluminescence from amorphous tantalum oxide films. Applied Physics Letters, 2006, 89, 021915.	1.5	72
23	Ag Nanorods Coated with Ultrathin TiO2 Shells as Stable and Recyclable SERS Substrates. Scientific Reports, 2015, 5, 15442.	1.6	72
24	High-Performance Real-Time SERS Detection with Recyclable Ag Nanorods@HfO <sub>2</sub> Substrates. ACS Applied Materials & Interfaces, 2016, 8, 27162-27168.	4.0	68
25	Preparation of MoO3nanostructures and their optical properties. Journal of Physics Condensed Matter, 2003, 15, L547-L552.	0.7	67
26	Origin of the defects-induced ferromagnetism in un-doped ZnO single crystals. Applied Physics Letters, 2013, 102, .	1.5	67
27	Nanogap effects on near- and far-field plasmonic behaviors of metallic nanoparticle dimers. Physical Chemistry Chemical Physics, 2015, 17, 29293-29298.	1.3	67
28	Low-temperature synthesis of large-scale arrays of aligned tungsten oxide nanorods. Journal of Physics Condensed Matter, 2003, 15, L453-L461.	0.7	65
29	Synthesis and optical properties of V2O5 nanorods. Journal of Chemical Physics, 2007, 126, 164701.	1.2	61
30	Hydrothermal fabrication of monoclinic bismuth vanadate (m-BiVO4) nanoparticles for photocatalytic degradation of toxic organic dyes. Materials Science and Engineering B: Solid-State Materials for Advanced Technology, 2019, 242, 83-89.	1.7	61
31	Enhanced field emission properties of MoO2 nanorods with controllable shape and orientation. Materials Letters, 2004, 58, 3812-3815.	1.3	60
32	Preparation and characterization of Vanadium pentoxide (V2O5) for photocatalytic degradation of monoazo and diazo dyes. Surfaces and Interfaces, 2020, 19, 100502.	1.5	60
33	Oxygen defect induced photoluminescence of HfO2 thin films. Applied Physics Letters, 2008, 93, .	1.5	59
34	Rapid recognition of isomers of monochlorobiphenyls at trace levels by surface-enhanced Raman scattering using Ag nanorods as a substrate. Nano Research, 2010, 3, 423-428.	5.8	59
35	Enhanced surface-enhanced Raman scattering performance by folding silver nanorods. Applied Physics Letters, 2012, 100, .	1.5	54
36	Facile synthesis of Zinc vanadate Zn3(VO4)2 for highly efficient visible light assisted photocatalytic activity. Journal of Alloys and Compounds, 2019, 775, 281-289.	2.8	52

#	Article	IF	CITATIONS
37	Enhanced photocatalytic activity of porous α-Fe <sub>2</sub> O <sub>3</sub> films prepared by rapid thermal oxidation. Journal Physics D: Applied Physics, 2008, 41, 202002.	1.3	50
38	Novel Ag–Cu substrates for surface-enhanced Raman scattering. Materials Letters, 2009, 63, 2306-2308.	1.3	50
39	Room-temperature ferromagnetism in un-doped ZrO <sub>2</sub> thin films. Journal Physics D: Applied Physics, 2013, 46, 445004.	1.3	50
40	The effect of underlayer thin films on the surface-enhanced Raman scattering response of Ag nanorod substrates. Applied Physics Letters, 2010, 97, .	1.5	49
41	Defects-Driven Ferromagnetism in Undoped Dilute Magnetic Oxides: A Review. Journal of Materials Science and Technology, 2015, 31, 969-978.	5.6	49
42	Novel [111] oriented Î <sup>3</sup> -Mo2N thin films deposited by magnetron sputtering as an anode for aqueous micro-supercapacitors. Electrochimica Acta, 2017, 245, 237-248.	2.6	48
43	Surface-enhanced Raman scattering from helical silver nanorod arrays. Chemical Communications, 2011, 47, 4466.	2.2	46
44	A Simple Model to Describe the Rule of Glancing Angle Deposition. Materials Transactions, 2011, 52, 469-473.	0.4	46
45	Self-assembled patterns of iron oxide nanoparticles by hydrothermal chemical-vapor deposition. Applied Physics Letters, 2001, 79, 4207-4209.	1.5	42
46	Synthesis and photoluminescence of aligned ZnO nanorods by thermal decomposition of zinc acetate at a substrate temperature of â^1⁄4250 °C. Journal Physics D: Applied Physics, 2005, 38, 3934-3937.	1.3	41
47	Nanoparticle-on-mirror cavity modes for huge and/or tunable plasmonic field enhancement. Nanotechnology, 2017, 28, 105203.	1.3	40
48	Detailed correlations between SERS enhancement and plasmon resonances in subwavelength closely spaced Au nanorod arrays. Nanoscale, 2018, 10, 4267-4275.	2.8	40
49	Pinhole-Containing, Subnanometer-Thick Al <sub>2</sub> O <sub>3</sub> Shell-Coated Ag Nanorods as Practical Substrates for Quantitative Surface-Enhanced Raman Scattering. Journal of Physical Chemistry C, 2016, 120, 606-615.	1.5	39
50	Effect of magnetic field on the visible light emission of V2O5 nanorods. Applied Physics Letters, 2009, 94, .	1.5	38
51	Indirect to direct band gap transition in ultra-thin silicon films. Physical Chemistry Chemical Physics, 2013, 15, 6063.	1.3	37
52	Fabrication of silver-coated silicon nanowire arrays for surface-enhanced Raman scattering by galvanic displacement processes. Applied Surface Science, 2009, 256, 916-920.	3.1	36
53	Substrate effect on the room-temperature ferromagnetism in un-doped ZnO films. Applied Physics Letters, 2012, 101, .	1.5	36
54	Detection of corrosion inhibitor adsorption via a surface-enhanced Raman spectroscopy (SERS) silver nanorods tape sensor. Sensors and Actuators B: Chemical, 2020, 321, 128617.	4.0	36

<

#	Article	IF	CITATIONS
55	Rapid detection of 2, 3, 3′, 4, 4′-pentachlorinated biphenyls by silver nanorods-enhanced Raman spectroscopy. Physica E: Low-Dimensional Systems and Nanostructures, 2010, 42, 1717-1720.	1.3	34
56	Enhanced photoelectrochemical properties of TiO <sub>2</sub> nanorod arrays decorated with CdS nanoparticles. Science and Technology of Advanced Materials, 2014, 15, 055006.	2.8	34
57	Tunable Lattice Coupling of Multipole Plasmon Modes and Near-Field Enhancement in Closely Spaced Gold Nanorod Arrays. Scientific Reports, 2016, 6, 23159.	1.6	34
58	Study of the interfacial charge transfer in bismuth vanadate/reduce graphene oxide (BiVO4/rGO) composite and evaluation of its photocatalytic activity. Research on Chemical Intermediates, 2020, 46, 1201-1215.	1.3	34
59	Efficient photocatalysis with graphene oxide/Ag/Ag <sub>2</sub> S–TiO <sub>2</sub> nanocomposites under visible light irradiation. RSC Advances, 2018, 8, 5784-5791.	1.7	33
60	Phase-dependent and defect-driven d <sup>0</sup> ferromagnetism in undoped ZrO <sub>2</sub> thin films. RSC Advances, 2015, 5, 3636-3641.	1.7	32
61	Fabrication and characterization of polycrystalline silicon nanowires with silver-assistance by electroless deposition. Applied Surface Science, 2011, 257, 3861-3866.	3.1	31
62	Dependence of the Thermal Conductivity of <mml:math xmlns:mml="http://www.w3.org/1998/Math/MathML" display="inline"&gt;<mml:mrow><mml:msub><mml:mrow><mml:mi>BiFeO</mml:mi></mml:mrow><mml:mrow> Thin Films on Polarization and Structure. Physical Review Applied, 2017, 8, .</mml:mrow></mml:msub></mml:mrow></mml:math 	<mm15 mm1:mn&gt;</mm15 	3 <del 31ml:mn><
63	Non-invasive disease diagnosis using surface-enhanced Raman spectroscopy of urine and saliva. Applied Spectroscopy Reviews, 2020, 55, 197-219.	3.4	31
64	Morphological effects on the photocatalytic performance of FeVO4 nanocomposite. Nano Structures Nano Objects, 2020, 22, 100431.	1.9	31
65	TiO2 nanorod arrays decorated with Au nanoparticles as sensitive and recyclable SERS substrates. Journal of Alloys and Compounds, 2021, 861, 157999.	2.8	31
66	Photocatalytic properties of TiO2 thin films obtained by glancing angle deposition. Applied Surface Science, 2012, 258, 2766-2770.	3.1	30
67	Universal Near-Field Interference Patterns of Fano Resonances in Two-Dimensional Plasmonic Crystals. Plasmonics, 2016, 11, 1377-1383.	1.8	30
68	Unexpected large nanoparticle size of single dimer hotspot systems for broadband SERS enhancement. Optics Letters, 2018, 43, 2332.	1.7	30
69	Contrastive Analysis of the Raman Spectra of Polychlorinated Benzene: Hexachlorobenzene and Benzene. Sensors, 2011, 11, 11510-11515.	2.1	29
70	Tuning the optical bandgap of TiO2-TiN composite films as photocatalyst in the visible light. AIP Advances, 2013, 3, .	0.6	29
71	From zinc nanowires to zinc oxide nanowires: a low substrate-temperature approach. Journal Physics D: Applied Physics, 2005, 38, 1068-1071.	1.3	28
72	Photocatalytic performance of ferric vanadate (FeVO4) nanoparticles synthesized by hydrothermal method. Materials Science in Semiconductor Processing, 2021, 129, 105785.	1.9	28

#	Article	IF	CITATIONS
73	Preparation of a superhydrophobic TiN/PTFE composite film toward self-cleaning and corrosion protection applications. Journal of Materials Science, 2021, 56, 1413-1425.	1.7	27
74	Optical Properties and Surface Enhanced Raman Scattering of L-Shaped Silver Nanorod Arrays. Journal of Physical Chemistry C, 2011, 115, 14131-14140.	1.5	26
75	MoO <sub><i>x</i></sub> thin films deposited by magnetron sputtering as an anode for aqueous micro-supercapacitors. Science and Technology of Advanced Materials, 2013, 14, 065005.	2.8	26
76	Flexible and adhesive tape decorated with silver nanorods for in-situ analysis of pesticides residues and colorants. Mikrochimica Acta, 2019, 186, 603.	2.5	26
77	Growth control of tungsten oxide nanostructures on planar silicon substrates. Applied Physics Letters, 2006, 89, 193111.	1.5	25
78	Nanostructuring HfO <sub>2</sub> Thin Films as Antireflection Coatings. Journal of the American Ceramic Society, 2009, 92, 3077-3080.	1.9	25
79	Synthesis and field emission property of VO2 nanorods with a body-centered-cubic structure. Physica E: Low-Dimensional Systems and Nanostructures, 2009, 41, 548-551.	1.3	25
80	The fabrication of large-scale sub-10-nm core-shell silicon nanowire arrays. Nanoscale Research Letters, 2013, 8, 405.	3.1	25
81	SERS detection and characterization of uranyl ion sorption on Âsilver nanorods wrapped with Al2O3 layers. Mikrochimica Acta, 2017, 184, 2775-2782.	2.5	25
82	Label-free surface-enhanced Raman spectroscopy of serum based on multivariate statistical analysis for the diagnosis and staging of lung adenocarcinoma. Vibrational Spectroscopy, 2019, 100, 177-184.	1.2	25
83	Enhanced photocatalytic properties of CdS nanoparticles decorated α-Fe2O3 nanopillar arrays under visible light. Journal of Colloid and Interface Science, 2017, 494, 107-113.	5.0	24
84	Al <sub>2</sub> O <sub>3</sub> Encapsulated Teflon Nanostructures with High Thermal Stability and Efficient Antireflective Performance. ACS Applied Materials & amp; Interfaces, 2017, 9, 36327-36337.	4.0	23
85	Highly stable and active SERS substrates with Ag–Ti alloy nanorods. Nanoscale, 2018, 10, 19863-19870.	2.8	23
86	Visible Light Driven Photoanodes for Water Oxidation Based on Novel r-GO/β-Cu2V2O7/TiO2 Nanorods Composites. Nanomaterials, 2018, 8, 544.	1.9	23
87	Bismuth vanadate/MXene (BiVO4/Ti3C2) heterojunction composite: enhanced interfacial control charge transfer for highly efficient visible light photocatalytic activity. Environmental Science and Pollution Research, 2021, 28, 35911-35923.	2.7	23
88	Mechanically robust antireflective coatings. Nano Research, 2018, 11, 1699-1713.	5.8	22
89	Robust quantitative SERS analysis with Relative Raman scattering intensities. Talanta, 2021, 221, 121465.	2.9	22
90	Molybdenum oxide film with stable pseudocapacitive property for aqueous micro-scale electrochemical capacitor. Electrochimica Acta, 2014, 134, 84-91.	2.6	21

#	Article	IF	CITATIONS
91	Tunable SERS-Tags-Hidden Gold Nanorattles for Theranosis of Cancer Cells with Single Laser Beam. Scientific Reports, 2015, 4, 6709.	1.6	21
92	Fast Surface Charge Transfer with Reduced Band Gap Energy of FeVO4/Graphene Nanocomposite and Study of Its Electrochemical Property and Enhanced Photocatalytic Activity. Arabian Journal for Science and Engineering, 2019, 44, 6659-6667.	1.7	21
93	TiN Nanorods as Effective Substrate for Surface-Enhanced Raman Scattering. Journal of Physical Chemistry C, 2019, 123, 29353-29359.	1.5	21
94	Latticing vertically aligned Ag nanorods to enhance its SERS sensitivity. Materials Research Bulletin, 2012, 47, 921-924.	2.7	20
95	Near-field mapping of three-dimensional surface charge poles for hybridized plasmon modes. AIP Advances, 2015, 5, .	0.6	20
96	Role of Ag2S coupling on enhancing the visible-light-induced catalytic property of TiO2 nanorod arrays. Scientific Reports, 2016, 6, 19754.	1.6	20
97	Hydrogen permeation properties of CrxCy@Cr2O3/Al2O3 composite coating derived from selective oxidation of a Cr C alloy and atomic layer deposition. International Journal of Hydrogen Energy, 2018, 43, 21133-21141.	3.8	20
98	Phase control and Young's modulus of tungsten thin film prepared by dual ion beam sputtering deposition. AIP Advances, 2018, 8, .	0.6	20
99	Facile synthesis of Zn3(VO4)2/FeVO4 heterojunction and study on its photocatalytic and electrochemical properties. Applied Nanoscience (Switzerland), 2020, 10, 421-433.	1.6	20
100	Construction of 1T-MoS <sub>2</sub> quantum dots-interspersed (Bi <sub>1â^'x</sub> Fe <sub>x</sub> )VO <sub>4</sub> heterostructures for electron transport and photocatalytic properties. RSC Advances, 2021, 11, 13105-13118.	1.7	20
101	Surface-enhanced Raman scattering from a hexagonal lattice of micro-patterns of vertically aligned Ag nanorods. Physica E: Low-Dimensional Systems and Nanostructures, 2011, 44, 460-463.	1.3	19
102	Growth of [010] oriented α-MoO <sub>3</sub> nanorods by pulsed electron beam deposition. Applied Physics Letters, 2011, 99, 223104.	1.5	19
103	Gradual plasmon evolution and huge infrared near-field enhancement of metallic bridged nanoparticle dimers. Physical Chemistry Chemical Physics, 2016, 18, 2319-2323.	1.3	19
104	Semi-quantitative analysis of multiple chemical mixtures in solution at trace level by surface-enhanced Raman Scattering. Scientific Reports, 2017, 7, 6186.	1.6	19
105	The Effect of Annealing Treatment and Atom Layer Deposition to Au/Pt Nanoparticles-Decorated TiO2 Nanorods as Photocatalysts. Molecules, 2018, 23, 525.	1.7	19
106	Synthesis and self-organization of γ-Fe2O3 nanoparticles by hydrothermal chemical vapor deposition. Materials Letters, 2005, 59, 3375-3377.	1.3	18
107	The synthesis and photoluminescence properties of selenium-treated porous silicon nanowire arrays. Nanotechnology, 2011, 22, 075203.	1.3	18
108	Quantitative Analysis of Single and Mix Food Antiseptics Basing on SERS Spectra with PLSR Method. Nanoscale Research Letters, 2016, 11, 296.	3.1	18

#	Article	IF	CITATIONS
109	Characterization of Fe nanorods grown directly from submicron-sized iron grains by thermal evaporation. Physical Review B, 2004, 70, .	1.1	16
110	Rapid Detection of Polychlorinated Biphenyls at Trace Levels in Real Environmental Samples by Surface-Enhanced Raman Scattering. Sensors, 2011, 11, 10851-10858.	2.1	16
111	Effects of Porosity and Temperature on Oxidation Behavior in Air of Selected Nuclear Graphites. Materials Transactions, 2012, 53, 1159-1163.	0.4	16
112	Enhanced room-temperature ferromagnetism in un-doped ZnO thin films by thermal annealing in a strong magnetic field. Journal of Applied Physics, 2012, 111, 103524.	1.1	16
113	Fabrication of TiN nanostructure as a hydrogen peroxide sensor by oblique angle deposition. Nanoscale Research Letters, 2014, 9, 105.	3.1	16
114	HfO <sub>2</sub> Nanorod Array as Highâ€Performance and Highâ€Temperature Antireflective Coating. Advanced Materials Interfaces, 2017, 4, 1600892.	1.9	16
115	HfO2-wrapped slanted Ag nanorods array as a reusable and sensitive SERS substrate for trace analysis of uranyl compounds. Sensors and Actuators B: Chemical, 2018, 265, 539-546.	4.0	16
116	Coupling between plasmonic nanohole array and nanorod array: the emerging of a new extraordinary optical transmission mode and epsilon-near-zero property. Journal Physics D: Applied Physics, 2020, 53, 275202.	1.3	16
117	Preparation and Photocatalytic Property of TiO <sub>2</sub> Columnar Nanostructure Films. Materials Transactions, 2011, 52, 1939-1942.	0.4	15
118	Enhancement of the photocatalytic property of TiO2 columnar nanostructured films by changing deposition angle. Materials Research Bulletin, 2014, 50, 68-72.	2.7	15
119	The Ti@MoOx nanorod array as a three dimensional film electrode for micro-supercapacitors. Electrochemistry Communications, 2014, 44, 23-26.	2.3	15
120	Sensitivity and Reusability of SiO2 NRs@ Au NPs SERS Substrate in Trace Monochlorobiphenyl Detection. Nanoscale Research Letters, 2015, 10, 444.	3.1	15
121	Well-aligned NiSi/Si heterostructured nanowire arrays as field emitters. Journal of Vacuum Science and Technology B:Nanotechnology and Microelectronics, 2015, 33, .	0.6	15
122	Analytical plasmon dispersion in subwavelength closely spaced Au nanorod arrays from planar metal–insulator–metal waveguides. Journal of Materials Chemistry C, 2017, 5, 6079-6085.	2.7	15
123	Quantification of trace chemicals in unknown complex systems by SERS. Talanta, 2018, 186, 452-458.	2.9	15
124	Photoluminescence of amorphous niobium oxide films synthesized by solid-state reaction. Thin Solid Films, 2008, 516, 4213-4216.	0.8	14
125	Anisotropic Ti x Sn1- x O2 nanostructures prepared by magnetron sputter deposition. Nanoscale Research Letters, 2011, 6, 326.	3.1	14
126	Enhanced light absorption of amorphous silicon thin film by substrate control and ion irradiation. Nanoscale Research Letters, 2014, 9, 173.	3.1	14

#	Article	IF	CITATIONS
127	Compositional Analysis of Ternary and Binary Chemical Mixtures by Surface-Enhanced Raman Scattering at Trace Levels. Nanoscale Research Letters, 2015, 10, 437.	3.1	14
128	Design of Ag nanorods for sensitivity and thermal stability of surface-enhanced Raman scattering. Nanotechnology, 2017, 28, 405602.	1.3	14
129	Bilayer SiO <sub>2</sub> Nanorod Arrays as Omnidirectional and Thermally Stable Antireflective Coating. Advanced Engineering Materials, 2018, 20, 1700942.	1.6	14
130	Simultaneous Thermal Stability and Ultrahigh Sensitivity of Heterojunction SERS Substrates. Nanomaterials, 2019, 9, 830.	1.9	14
131	Design of Armrest Ag Nanorod Arrays with High SERS Performance for Sensitive Biomolecule Detection. Journal of Physical Chemistry C, 2020, 124, 21054-21062.	1.5	14
132	Facile Synthesis of α-Fe <sub>2</sub> O <sub>3</sub> Nanostructured Films with Controlled Morphology. Materials Transactions, 2009, 50, 1351-1354.	0.4	13
133	CO <sub>2</sub> corrosion of IG-110 nuclear graphite studied by gas chromatography. Journal of Nuclear Science and Technology, 2014, 51, 487-492.	0.7	13
134	Tunable field emission properties of well-aligned silicon nanowires with controlled aspect ratio and proximity. RSC Advances, 2014, 4, 31729-31734.	1.7	13
135	Synthesis of novel visible light assisted Pt doped zinc vanadate (Pt/Zn4V2O9) for enhanced photocatalytic properties. Chemical Physics, 2020, 539, 110980.	0.9	13
136	Facile synthesis of Se/BiVO4 heterojunction composite and evaluation of synergetic reaction mechanism for efficient photocatalytic staining of organic dye pollutants in wastewater under visible light. Journal of Materials Science: Materials in Electronics, 2020, 31, 19599-19612.	1.1	13
137	Quantum sieving of H <sub>2</sub> /D <sub>2</sub> in MOFs: a study on the correlation between the separation performance, pore size and temperature. Journal of Materials Chemistry A, 2020, 8, 6319-6327.	5.2	13
138	Fabrication of MoO <i><sub>x</sub></i> Film as a Conductive Anode Material for Micro-Supercapacitors by Electrodeposition and Annealing. Journal of the Electrochemical Society, 2014, 161, A1051-A1057.	1.3	12
139	Fabrication and simulation of V-shaped Ag nanorods as high-performance SERS substrates. Physical Chemistry Chemical Physics, 2018, 20, 25623-25628.	1.3	12
140	Direct observation of fast surface dynamics in sub-10-nm nanoglass particles. Applied Physics Letters, 2019, 114, 043103.	1.5	12
141	Ag Nanorods-Based Surface-Enhanced Raman Scattering: Synthesis, Quantitative Analysis Strategies, and Applications. Frontiers in Chemistry, 2019, 7, 376.	1.8	12
142	Control the relative length of carbon nanotubes from site to site on one silicon substrate. Applied Physics Letters, 2005, 87, 223121.	1.5	11
143	Ion-implantation-induced patterns formation on silicon substrates. Physica E: Low-Dimensional Systems and Nanostructures, 2009, 41, 833-837.	1.3	11
144	Mechanical property improvement by texture control of magnetron co-sputtered Zr-Ti films. Journal of Applied Physics, 2014, 115, .	1.1	11

#	Article	IF	CITATIONS
145	Effect of Xe ion irradiation on photocatalytic performance of oblique TiO2 nanowire arrays. Applied Surface Science, 2015, 327, 478-482.	3.1	11
146	Annealing effect on the photoelectrochemical and photocatalytic performance of TiO <sub>2</sub> nanorod arrays. RSC Advances, 2017, 7, 51382-51390.	1.7	11
147	Microstructure evolution and Young's modulus of He-implanted nanocrystalline tungsten film. Journal of Nuclear Materials, 2019, 518, 226-233.	1.3	11
148	Oxygen deficient V2O5 nanorods for gas sensing. Physica E: Low-Dimensional Systems and Nanostructures, 2011, 43, 1726-1729.	1.3	10
149	Pinhole Effect on the Melting Behavior of Ag@Al2O3 SERS Substrates. Nanoscale Research Letters, 2016, 11, 170.	3.1	10
150	Large-Area Fabrication of Complex Nanohole Arrays with Highly Tunable Plasmonic Properties. ACS Applied Materials & Interfaces, 2020, 12, 37435-37443.	4.0	10
151	Self-networking of carbon nanotubes. Chemical Communications, 2002, , 962-963.	2.2	9
152	Synthesis of silicon carbide nanowires by solid phase source chemical vapor deposition. Frontiers of Materials Science in China, 2007, 1, 304-308.	0.5	9
153	Visible Light Photoelectrochemical Properties of N-Doped TiO2Nanorod Arrays from TiN. Journal of Nanomaterials, 2013, 2013, 1-8.	1.5	9
154	Direct observation of heavy quasiparticles in the Kondo-lattice compound <mml:math xmlns:mml="http://www.w3.org/1998/Math/MathML"&gt;<mml:mrow><mml:mi>Cel</mml:mi><mml:msub><mml:r mathvariant="normal"&gt;n<mml:mn>3</mml:mn></mml:r </mml:msub></mml:mrow>. Physical Review B, 2018, 97, .</mml:math 	ni 1.1	9
155	Amorphous magnetic semiconductors with Curie temperatures above room temperature. Journal of Semiconductors, 2019, 40, 081510.	2.0	9
156	Effects of Ti transition layers and thermal annealing on the adhesive property of Ag nanorods-based SERS sensors. Applied Surface Science, 2019, 476, 363-368.	3.1	9
157	Realignment of slanted Fe nanorods on silicon substrates by a strong magnetic field. Nano Research, 2010, 3, 438-443.	5.8	8
158	The Nanofabrication and Application of Substrates for Surface-Enhanced Raman Scattering. International Journal of Spectroscopy, 2012, 2012, 1-7.	1.4	8
159	Photocatalytic Properties of Columnar Nanostructured <mml:math xmlns:mml="http://www.w3.org/1998/Math/MathML"&gt; <mml:mrow> <mml:msub> <mml:mrow> <mml:mtext>TiO <mathvariant="bold"> 2  </mathvariant="bold"></mml:mtext></mml:mrow></mml:msub> </mml:mrow> Films Fabricated by Sputtering Ti and Subsequent Annealing. Advances in Materials Science and Engineering. 2012. 2012. 1-5.</mml:math 	«/mml:mt 1.0	extz
160	Three-dimensional bulk electronic structure of the Kondo lattice CeIn3 revealed by photoemission. Scientific Reports, 2016, 6, 33613.	1.6	8
161	Ag Nanorods-Oxide Hybrid Array Substrates: Synthesis, Characterization, and Applications in Surface-Enhanced Raman Scattering. Sensors, 2017, 17, 1895.	2.1	8
162	Research progress of SERS on uranyl ions and uranyl compounds: a review. Journal of Materials Chemistry C, 2022, 10, 4006-4018.	2.7	8

#	Article	IF	CITATIONS
163	Fabrication and Optical Property of Periodic <mml:math xmlns:mml="http://www.w3.org/1998/Math/MathML"&gt;<mml:msub><mml:mrow><mml:mtext>Sn</mml:mtext> Patterned by the Polystyrene Mic. Journal of Nanomaterials, 2011, 2011, 1-7.</mml:mrow></mml:msub></mml:math 	<b m.ឆl:m	row <b>⁊ &lt; mml:m</b> ro
164	α-Fe <sub>2</sub> O <sub>3</sub> nanopillar arrays fabricated by electron beam evaporation for the photoassisted degradation of dyes with H <sub>2</sub> O <sub>2</sub> . RSC Advances, 2016, 6, 534-540.	1.7	7
165	Efficient Hydrogen Evolution Reaction on Ni3S2 Nanorods with a P/N Bipolar Electrode Prepared by Dealloying Sulfurization of NiW Amorphous Alloys. ACS Applied Energy Materials, 2020, 3, 5745-5755.	2.5	7
166	A high-strength Co–Fe–Ta–B metallic-glass phase enabled tensile plasticity in Co–Fe–Ta–B–O ox glass matrix nanocomposites. Applied Physics Letters, 2020, 116, .	de <sub>1.5</sub>	7
167	Magnetic and Microwave Absorption Properties of Core/Shell FeCo-Based Nanocomposites Synthesized by a Simple Wet Chemical Method. IEEE Transactions on Magnetics, 2011, 47, 3456-3459.	1.2	6
168	Atomic oxygen treatment effects on magnetron sputtered Zr–Ti binary films. Applied Surface Science, 2015, 324, 669-676.	3.1	6
169	Large lattice mismatch induced perpendicular magnetic anisotropy and perpendicular exchange bias in CoPt/FeMn bilayer films. Science China Technological Sciences, 2019, 62, 2009-2013.	2.0	6
170	The effect of nanorod position on the plasmonic properties of the complex nanorod in nanohole arrays. Journal Physics D: Applied Physics, 2021, 54, 155201.	1.3	6
171	Coupling between Surface Plasmon Modes of Single-Layer Complex Silver Nanohole Arrays and Enhancing Index Sensing. ACS Applied Nano Materials, 2022, 5, 9761-9770.	2.4	6
172	Selecting the growth sites of carbon nanotubes on silicon substrates by ion implantation. Applied Physics Letters, 2006, 88, 263115.	1.5	5
173	The Influence of Pores on Irradiation Property of Selected Nuclear Graphites. Advances in Materials Science and Engineering, 2012, 2012, 1-6.	1.0	5
174	Omnidirectional SiO2 AR Coatings. Coatings, 2018, 8, 210.	1.2	5
175	Standing wave type localized surface plasmon resonance of multifold Ag nanorods. Nanotechnology, 2019, 30, 055703.	1.3	5
176	Platinum doped bismuth vanadate (Pt/BiVO4) for enhanced photocatalytic pollutant degradation using visible light irradiation. Journal of Materials Science: Materials in Electronics, 2022, 33, 15116-15131.	1.1	5
177	Preparation of Highly Textured ZnO Thin Films by Pulsed Electron Deposition. Materials Transactions, 2011, 52, 1764-1767.	0.4	4
178	Slanted Ag-Al alloy nanorods arrays for highly active and stable surface-enhanced Raman scattering substrates. Nanotechnology, 2019, 30, 235703.	1.3	4
179	Highly Conductive Nanograting–Nanohole Structures with Tunable and Dual-Band Spectral Transparency. ACS Applied Electronic Materials, 2021, 3, 3489-3500.	2.0	4
180	The Regulation of Surface-Enhanced Raman Scattering Sensitivity of Silver Nanorods by Silicon Sections. Journal of Nanomaterials, 2013, 2013, 1-5.	1.5	3

#	Article	IF	CITATIONS
181	Facile decolorization of methylene blue with flower-like manganese wads. Water Science and Technology, 2014, 69, 1094-1100.	1.2	3
182	200 keV Xe+ ions irradiation effects on Zr–Ti binary films. Nuclear Instruments & Methods in Physics Research B, 2015, 350, 26-31.	0.6	3
183	Zigzag Localized Surface Plasmon Resonance Wavelength Shift of Asymmetric V-Shape Ag Nanorods. Journal of Physical Chemistry C, 2018, 122, 17400-17405.	1.5	3
184	Fishnet-like Ni–Fe–N co-modified graphene aerogel catalyst for highly efficient oxygen reduction reaction in an alkaline medium. Journal of Applied Electrochemistry, 2019, 49, 1211-1226.	1.5	3
185	Formation and Properties of Amorphous Multi-Component (CrFeMoNbZr)Ox Thin Films. Metals, 2020, 10, 599.	1.0	3
186	From carbon nanotube crystals to carbon nanotube flowers. Tsinghua Science and Technology, 2005, 10, 741-744.	4.1	2
187	Selective growth of graphite micro-rods with SiO2 nanowire cores by chemical vapor deposition. Applied Physics Letters, 2006, 88, 113102.	1.5	2
188	Irradiation Induced Localized Amorphization in Mo-Re Alloy Films. Materials Transactions, 2010, 51, 670-674.	0.4	2
189	Thermal Stability of HfO <sub>2</sub> Nanostructures as Antireflection Coatings. Nanoscience and Nanotechnology Letters, 2011, 3, 731-734.	0.4	2
190	X-ray irradiation-induced reversible wettability modification of titanium NRAs. RSC Advances, 2015, 5, 4524-4528.	1.7	2
191	Enhanced Visible Light Photocatalytic Performance by Nanostructured Semiconductors with Glancing Angle Deposition Method. , 0, , .		2
192	Electrochemical Materials Design for Micro-Supercapacitors. , 0, , .		2
193	Glancing angle deposition of Fe triangular nanoprisms consisting of vertically-layered nanoplates. Journal of Crystal Growth, 2016, 451, 113-119.	0.7	2
194	Anisotropic ferromagnetism in Fe x Sn1â^'x O2 nanostructure arrays. Journal of Materials Science, 2018, 53, 3280-3288.	1.7	2
195	The evolution of He+ irradiation-induced point defects and helium retention in nuclear graphite. Journal of Nuclear Science and Technology, 2019, 56, 744-751.	0.7	2
196	Strong long-range perpendicular exchange bias across a spacer layer. AIP Advances, 2019, 9, 125046.	0.6	2
197	Performance of Transparent Metallic Thin Films. Journal of Physical Chemistry C, 2021, 125, 16334-16342.	1.5	2
198	Tailoring TiO <sub>2</sub> /Al <sub>2</sub> O <sub>3</sub> heterolayers as optical filters for the visible region. Nanoscale Advances, 2022, 4, 1608-1616.	2.2	2

#	Article	IF	CITATIONS
199	GROWTH CARBON NANOTUBES DIRECTLY ON PRISTINE SILICON SUBSTRATES. International Journal of Nanoscience, 2006, 05, 433-438.	0.4	1
200	Influence of deposition conditions on the morphology and phase of tungsten oxide nanorods synthesized by thermal oxidation. Frontiers of Materials Science in China, 2007, 1, 16-19.	0.5	1
201	The Novel Wetting Behavior of Periodic Ti <i><sub>x</sub></i> Sn <sub>1−</sub> <i><sub>x</sub></i> O <sub>2</sub> Nanostructures. Materials Transactions, 2012, 53, 191-194.	0.4	1
202	Synthesis of flower-like manganese wad and its decolorization performance for azo dye Congo red. Chemical Research in Chinese Universities, 2014, 30, 306-309.	1.3	1
203	Wettability manipulation of magnetic transition metal nanorod arrays by X-ray irradiation. Frontiers of Materials Science, 2015, 9, 311-315.	1.1	1
204	High-magnetic field annealing effect on room-temperature ferromagnetism enhancement of un-doped HfO2 thin films. Applied Physics A: Materials Science and Processing, 2015, 119, 917-921.	1.1	1
205	Mechanical properties and structure evolution of single-crystalline silicon irradiated by 1â€MeV Au+ and Cu+ ions. Nuclear Instruments & Methods in Physics Research B, 2018, 423, 75-81.	0.6	1
206	Surface-enhanced ZnS:Ag quantum dots scintillator. AIP Advances, 2019, 9, 105211.	0.6	1
207	Nanometer-Thick Al <sub>2</sub> O <sub>3</sub> Layers on Ag–Al Nanostructures as Conductive Electrodes. ACS Applied Nano Materials, 2021, 4, 1270-1281.	2.4	1
208	Microstructure and Properties of Pure Zirconium After Irradiation by Charged Particles. Thirty Years of Astronomical Discovery With UKIRT, 2013, , 417-426.	0.3	1
209	Thermal stability and sputtering resistance under irradiation of yttria dispersed ferrum films. Rare Metals, 2011, 30, 258-261.	3.6	Ο
210	Influence of vacuum annealing and irradiation on magnetic properties of Fe-3%Y2O3 films. Rare Metals, 2011, 30, 453-457.	3.6	0
211	Effects of Alkali Corrosion Preprocessing on the Growth of Aligned Silver Nanorods Array and Its Improvement for Surface-Enhanced Raman Scattering. Materials Transactions, 2012, 53, 1278-1281.	0.4	Ο
212	Rapid Detection and Recognition of Organic Pollutants at Trace Levels by Surface-Enhanced Raman Scattering. , 2012, , .		0
213	The Detection of Organic Pollutants at Trace Level by Variable Kinds of Silver Film with Novel Morphology. , 0, , .		Ο
214	Synthesis of nitrogen-doped reduced graphene oxide as metal-free electrocatalyst for oxygen reduction reactions. International Journal of Nanomanufacturing, 2016, 12, 252.	0.3	0
215	Preparation of TiO <sub align="right">2 nanorod arrays decorated with CdS nanoparticles exhibiting enhanced photoelectrochemical and photocatalytic properties in visible light. International Journal of Nanomanufacturing, 2016, 12, 237.</sub>	0.3	0
216	Antireflective Coatings: HfO <sub>2</sub> Nanorod Array as Highâ€Performance and Highâ€Temperature Antireflective Coating (Adv. Mater. Interfaces 6/2017). Advanced Materials Interfaces, 2017, 4, .	1.9	0

#	Article	IF	CITATIONS
217	AMORPHIZATION OF CERIUM MONONITRIDE DURING OXIDIZATION CHARACTERIZED BY OPTICAL MICROSCOPY, SCANNING ELECTRON MICROSCOPY, X-RAY DIFFRACTION AND X-RAY PHOTOELECTRON SPECTROSCOPY. Surface Review and Letters, 2019, 26, 1850180.	0.5	0
218	The IR plasmonic properties of sub-wavelength ITO rod arrays predicted by anisotropic effective medium theory. Nanotechnology, 2020, 31, 075203.	1.3	0
219	Design and fabrication of nanorod in nanohole arrays with highly tunable enhanced optical transmission. , 2021, , .		Ο
220	10.1063/1.5143598.2. , 2020, , .		0